Heliyon 9 (2023) e16922

Contents lists available at ScienceDirect

Heliyon

journal homepage: www.cell.com/heliyon

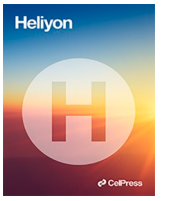

The mechanism of action and biodistribution of a novel EGFR/VEGF bispecific fusion protein that exhibited superior antitumor activities

Lan Deng, Lihua Wang, Jinzhao Zhang, Le Zhao, Yun Meng, Jidai Zheng, Wei Xu, Zhenping Zhu, Haomin Huang *

Sunshine Guojian Pharmaceutical (Shanghai) Co. Ltd. a 3SBio Inc. Company, 399 Libing Road, Shanghai, 201203, China

ARTICLE INFO

Keywords:
EGFR
VEGF
Biodistribution
VEGFR inhibitor
Endocytosis
Anticancer therapy

ABSTRACT

Despite the promising clinical benefits of therapies targeting epidermal growth factor receptor (EGFR) or vascular endothelial growth factor (VEGF) with antibodies in various cancers, resistance to these therapies will inevitably develop following treatment. Recent studies suggest that crosstalk between the EGFR and VEGF signaling pathways might be involved in the development of resistance. Therefore, simultaneous blockade of EGFR and VEGF signaling may be able to counteract this resistance and improve clinical outcomes. Here, we devised a fusion protein with two copies of VEGFR1 domain 2 connected to the C-terminus of cetuximab that can simultaneously bind to EGFR and VEGF and effectively inhibit target cell growth mediated by these two pathways. Furthermore, the fusion protein could bring soluble VEGF into target cells for degradation through internalization upon binding to EGFR. Tissue distribution in mice confirmed that the fusion protein effectively accumulated in tumors compared to its mAb counterpart cetuximab. These features resulted in stronger antitumor efficacies *in vivo* than the combination of bevacizumab and cetuximab. Thus, we provide a promising new strategy for the treatment of EGFR-overexpressing cancers.

1. Introduction

Epidermal growth factor receptor (EGFR) plays key roles in cell growth and development [1] and is overexpressed in many types of cancers, including lung cancer, colorectal cancer (CRC), breast cancer, head and neck cancer, ovarian cancer, pancreatic cancer, and glioblastoma [2]. Thus, EGFR overexpression and the dysregulation of EGFR signaling pathways are thought to promote tumorigenesis [3]. EGFR-targeting therapies, including EGFR tyrosine kinase inhibitors (TKIs) and monoclonal antibodies (mAbs), have been developed and are recommended for the treatment of metastatic lung cancer and colorectal cancer [4–8]. Although targeting EGFR initially results in progression-free survival (PFS) benefits and increases the objective response rate (ORR) in the clinic, patients inevitably develop resistance to EGFR-targeting agents [9–11]. As a result, the 5-year survival rate for patients with EGFR-mutant metastatic lung cancer is less than 15% [12]. Thus, it is urgent to develop novel therapeutic strategies to improve the treatment of EGFR-expressing cancers.

Evidence suggests that resistance to *anti*-EGFR therapies is at least partly due to vascular endothelial growth factor (VEGF)-

* Corresponding author.
E-mail address: huanghaomin@3s-guojian.com (H. Huang).

https://doi.org/10.1016/j.heliyon.2023.e16922
Received 21 February 2023; Received in revised form 18 May 2023; Accepted 1 June 2023
Available online 3 June 2023

mediated angiogenesis [13,14]. Angiogenesis is the formation of new blood vessels from the existing vasculature and is predominantly regulated by the VEGF family members VEGF-A, VEGF-B, VEGF-C and VEGF-D [15]. VEGF-A is a key stimulator of blood vessel formation in adult tissues, including tumors, whereas the other three members specifically regulate angiogenesis in embryonic or lymphatic tissues [16,17]. VEGF-A primarily signals through VEGF receptor 1 (Flt-1) and VEGF receptor 2 (Flk-1 or KDR). Although increasing evidence suggests that VEGF receptor 2 is the major receptor associated with endothelial cell proliferation and plays important roles in regulating mitogenic and angiogenic development [18,19], the affinity of VEGF receptor 1 for VEGF is 10-fold higher than that of VEGF receptor 2, and it was suggested that VEGF receptor 1 may reduce the number of unbound circulating VEGF molecules available to VEGF receptor 2 [20]. The extracellular domains (ECDs) of both VEGF receptor 1 (VEGFR1) and 2 (VEGFR2) consist of 7 immunoglobulin-like regions that bind to VEGF. Interestingly, it was reported that domain 2 of VEGFR1 (D2) binds to VEGF with an equilibrium dissociation constant (KD) of approximately 1.4 nM [21], while fusion proteins containing D2 can bind to VEGF and prevent the binding of VEGF to VEGFR2. VEGF that is released by tumor cells promotes angiogenesis to sustain tumor growth. Thus, blocking VEGF/VEGFR2 with mAbs and tyrosine kinase inhibitors has been shown to inhibit tumor growth in preclinical and clinical studies [22–27]. However, tumors often acquire resistance to *anti*-VEGF therapies following VEGF inhibition treatment, since tumors can develop redundant proangiogenic pathways to compensate for the loss of function of the VEGF/VEGFR2 pathway as the disease progresses [28]. Interestingly, it has been suggested that inhibiting EGFR signaling renders EGFR-expressing tumors sensitive to antiangiogenic therapies [29,30]. Thus, combining EGFR signaling inhibition with the suppression of angiogenesis via VEGF/VEGFR2 blockade might improve the outcomes of using mAb monotherapies to treat EGFR-expressing tumors [31,32].

In this study, we constructed a bifunctional fusion protein by fusing VEGFR1 D2 to the C-terminus of the *anti*-EGFR mAb cetuximab. The fusion protein (ED2) could bind to both EGFR and VEGF simultaneously and inhibit EGFR-overexpressing tumor cell growth and human endothelial cell growth. Importantly, ED2 could induce cellular uptake of VEGF in complex with the fusion protein for lysosome-mediated degradation. Furthermore, ED2 accumulated in EGFR-overexpressing tumors as effectively as its mAb counterparts, including cetuximab, in mice. As a result, ED2 exhibited more potent antitumor effects *in vivo* than the two mAb counterparts alone or in combination. In summary, combining cetuximab with D2 as a VEGF-targeting moiety is a promising strategy to exert therapeutic effects on EGFR-overexpressing cancers.

2. Materials and methods

2.1. Cell culture

The EGFR-overexpressing epidermal cell lines, A431 cells (ATCC, Cat#: CRL-1555) and SW48 cells (ATCC, Cat#: CCL-231) were cultured in RPMI-1640 (Gibco, Cat#:11875119) with 10% FBS and 1% penicillin/streptomycin in a humidified CO_2 incubator at 37 °C. The EGFR expressing breast cancer cell line MDA-MB-231 (ATCC, Cat#:HTB-26) and JIMT-1 (Nanjing Cobioer Biosciences Co. LTD, Cat#:CBP60378) were cultured in DMEM (Gibco, Cat#:11965092) with 10% FBS and 1% penicillin/streptomycin (P/S) in a humidified CO_2 incubator at 37 °C. FreeStyle™ 293F cells (Thermo Fisher, Cat#: R79007) were cultured in FreeStyle 293 medium (Gibco, Cat#:12338018) with 1% penicillin/streptomycin. KDR/NFAT-RE HEK293 cells (Promega, Cat#:GA2001) were cultured in DMEM (Gibco, Cat#:10569010) with 10% FBS and 1% penicillin/streptomycin.

2.2. Proliferation assay

A431 cells were seeded (5000 cells/well) in a 96-well culture plate in RPMI-1640 + 1% FBS and incubated overnight at 37 °C with 5% CO_2. The next day, the cells were incubated with serially diluted *anti*-EGFR × D2 fusion protein or cetuximab ranging from 5 pM to 100 nM in a final volume of 200 μl/well. The plates were incubated at 37 °C for 3 days, and cell viability was assessed using a CellTiter-Glo® Luminescent Cell Viability Assay (Promega, Cat#: G7570) according to the manufacturer's instructions.

2.3. Protein expression and purification

The construct expressing the *anti*-EGFR × D2 fusion protein was generated using the pcDNA3.4 vector (Thermo Fisher, Cat#: A14697). Transient transfection was performed by cotransfecting expression vectors encoding a heavy chain or a light chain individually into FreeStyle™ HEK293-F cells using 1 μg/ml 25 KDa linear polyethylenimine (Polysciences, Inc. Cat#:23966-1). One day after transfection, valproic acid (Sigma, Cat#: P4543-10G) was added to the culture at a final concentration of 3 mM. On day 2 posttransfection, medium containing 10% GlutaMAX, 10% 400 g/L glucose and 80% freestyle 293 medium was added to the cell culture as 10% of the total volume. Conditioned medium was collected 5–6 days after transient transfection. Antibodies in the culture media were purified by MabSelect SuRe affinity columns (GE Healthcare) on an AKTA Avant 25 fast protein liquid chromatography (FPLC) system. The columns were equilibrated with buffer A (25 mM sodium phosphate, 150 mM sodium chloride, pH = 7.0) prior to use. The culture media containing antibodies were then applied to the columns and eluted with Buffer B (100 mM sodium citrate, pH 3.5) to collect the desired proteins. The collected proteins were neutralized with 1 M Tris (pH 9.0) and then dialyzed against phosphate-buffered saline (PBS). Finally, the purity of the samples was analyzed by size exclusion chromatography-high-performance liquid chromatography (SEC-HPLC).

2.4. Enzyme-linked immunosorbent assay (ELISA)

The 96-well microplates were coated with 20 ng/well His-tagged EGFR or VEGF. The plates were washed with PBS containing 0.05% Tween-20 (PBST), blocked for 1 h with PBST containing 1% bovine serum albumin (BSA), and then incubated with serial dilutions of various antibodies for 1 h at room temperature. The plates were washed three times with PBST for 5 min and incubated with goat anti-human IgG (Fc specific and highly cross adsorbed) conjugated to horseradish peroxidase (HRP; Sigma, Cat#: P8375) for 1 h at room temperature. The plates were washed, and the reaction was developed with the chromogenic substrate tetramethylbenzidine for 2–3 min. The plates were then read on a SpectraMax 190 reader (Molecular Devices) at 450 nm. A similar protocol was used for the bridging ELISA. Briefly, the plates were coated with 20 ng/well VEGF after being blocked and incubated with threefold serial dilutions of antibodies for 1 h at 37 °C. The plates were then washed three times and incubated with 2 μg/ml His-tagged EGFR for 1 h at 37 °C. After being washed, an HRP-conjugated anti-6 × HisTag mAb (Invitrogen, Cat#:MA1-21315) was added, and the plates were incubated for 1 h at 37 °C. Then, the plates were measured as described above.

2.5. Surface plasmon resonance (SPR)

Antibody affinities were measured at room temperature using a Biacore 8K equipped with Protein A sensor chips (GE Healthcare). Briefly, antibodies flowing in HBS-EP + buffer (GE Healthcare) were first captured by the protein A chips. Varying concentrations of recombinant EGFR or VEGF were then injected at a flow rate of 30 μl/min. Sensorgrams were generated for each concentration, and the binding kinetics were analyzed using Biacore 8K Evaluation Software with a 1:1 Langmuir-binding model.

2.6. Flow cytometric analysis of A431 cells

To measure the ED2 protein binding affinity for EGFR-overexpressing cells, A431cells (3×10^5) were incubated with 3-fold serial dilutions of ED2 ranging from 0.23 nM to 500 nM in 200 μL of serum-free RPMI 1640 at 4 °C for 1 h. The cells were washed three times with PBS, and FITC-conjugated anti-human IgG (Sigma) was added and incubated at 4 °C for 30 min. The cells were washed and resuspended in 200 μL of PBS and analyzed by FACS (Beckman, Cytoflex).

2.7. KDR/NFAT-RE cell-based assay

KDR/NFAT-RE HEK293 cells (Promega, Cat#:GA2001) were engineered to express Luc2P under the control of the NFAT response element, as well as exogenous KDRs. Assays were performed according to the manufacturer's instructions. Briefly, KDR/NFAT-RE cells were seeded at 4×10^4 cells/well in 50 μl in white 96-well plates. Then, 25 μl of 3× serially diluted antibodies in DMEM containing 10% FBS and 30 ng/ml VEGF was added to the plates and incubated in a 37 °C humidified incubator with 5% CO_2 for 6 h. Then, 75 μl of Bio-Glo™ Reagent was added to each well, and the plates were incubated at room temperature for 5–30 min. Luminescence was measured on a SpectraMax i3x.

2.8. VEGF internalization by A431 cells

Prior to use, VEGF165 was labeled with Alexa Fluor™ 488 NHS Ester (Invitrogen) according to the manufacturer's instructions. A431 tumor cells were labeled with 50 nM LysoTracker Red DND-99 (Invitrogen) for 10 min, and then the buffer was replaced with fresh RPMI 1640 medium (Gibco) containing 10 μg/ml 488-labeled VEGF165 and 10 μg/ml the *anti*-EGFR x D2 fusion protein (Panel A) or cetuximab + bevacizumab (Panel B). Images of A431 cells were visualized with a PerkinElmer High-Content Analysis System (Operetta CLS).

2.9. Western blotting

SW48 or MDA-MB-231 cells were cultured in 6-well culture plates at 70% confluence overnight. Next day, the medium was replaced with DMEM medium containing 10% FBS + 1% P/S, and cells were treated with 20 ng/ml EGF, 400 ng/ml VEGF or the combination of EGF (20 ng/ml) with VEGF (400 ng/ml) for 5 h at 37 °C, respectively, prior to being lysed in NuPAGE LDS sample buffer (Invitrogen, Cat#NP0008). In the case of antibody treatments, tumor cells were treated with cetuximab, bevacizumab or ED2 (50 μM each) in the presence of both EGF (20 ng/ml) and VEGF (400 ng/ml) for 24 h at 37 °C prior to lysis, respectively. Western blotting was performed using standard procedures to detect the following bio-markers (these antibodies were all purchased from Cell Signal Technology): p44/42 MAPK (ERK1/2, Cat#:4695), phospho-p44/42 MAPK (ERK1/2, Thr202/Tyr204, Cat#:4370), AKT (Cat#:4691), phospho-AKT (Ser473, Cat#:4060), EGFR (Cat#:4267), phospho-EGFR (Tyr1086, Cat#:2220), VEGFR2 (Cat#:9698), phospho-VEGFR2 (Tyr1175, Cat#:3770), β-Actin (Cat#:3700).

2.10. Tissue biodistribution by ImmunoPET/CT

mAbs were modified with a novel bifunctional derivative of the chelate DFO (DBN) via a thiourea linkage and subsequently labeled with the zirconium-89 chelator (^{89}Zr). ^{89}Zr-mAbs were injected into BALB/c-nude mice (Beijing Vital River Laboratory Animal Technology Co., Ltd., strain #: 401) bearing SW48 xenograft tumors at a dose of 25 mg/kg. At 4 h, 24 h and 120 h postinjection, the

mice were anesthetized with 1.5% isoflurane/oxygen and scanned by CT and PET for 10 min. After PET/CT scanning, the percentage of injected dose per gram (%ID/g) in the brain, heart, liver, spleen, lung, kidney, muscle and tumor was calculated by P_{mod} (version 4.104). The CT and PET scans were coregistered using IAW 2.0.

2.11. Animal tumor models

Animal care and *in vivo* experiments were approved by the IACUC of Sunshine Guojian Pharmaceutical (Shanghai) Co. Ltd. and performed according to approved protocols (approval codes for SW48 and JIMT-1 xenograft model: AS-2021-155 and AS-2021-157). A human colon carcinoma SW48 xenograft tumor model and a human trastuzumab-resistant breast cancer JIMT-1 xenograft tumor model were established in female BALB/c nude (CAnN.Cg-Foxn1 nu/Crl) athymic mice, age 6–8 weeks, 18–20 g bodyweight (Beijing Vital River Laboratory Animal Technology Co., Ltd., strain #: 401) by subcutaneous inoculation of 5×10^6 SW48 or JIMT-1 tumor cells mixed with 50% Matrigel into the right flank. After tumor volume reached approximately 200 mm^3 and animals with too large or too small xenograft tumor were excluded, 40 of 50 tumor-bearing animals were randomly divided into groups (8 mice/group) and i.p. injected three times per week (4 weeks in total). Tumor volume was measured twice per week and calculated using the following formula: $V = LW^2/2$ (where V = volume, L = length and W = width). Mouse body weight (g) was measured at the indicated time points. The animal studies were repeated 3 times (n = 3).

3. Results

3.1. Construction of the anti-EGFR-D2 bifunctional fusion protein

To construct a molecule to simultaneously target EGFR and VEGF, we fused domain 2 of the VEGF receptor 1 (D2) to the C-terminus of the heavy chain of cetuximab via a (G4S) x 3 linker and coexpressed the modified heavy chain with the light chain of cetuximab (Fig. 1a). The fusion protein (ED2) was expressed in 293HEK cells and could be easily obtained as 98% monomeric products after one-

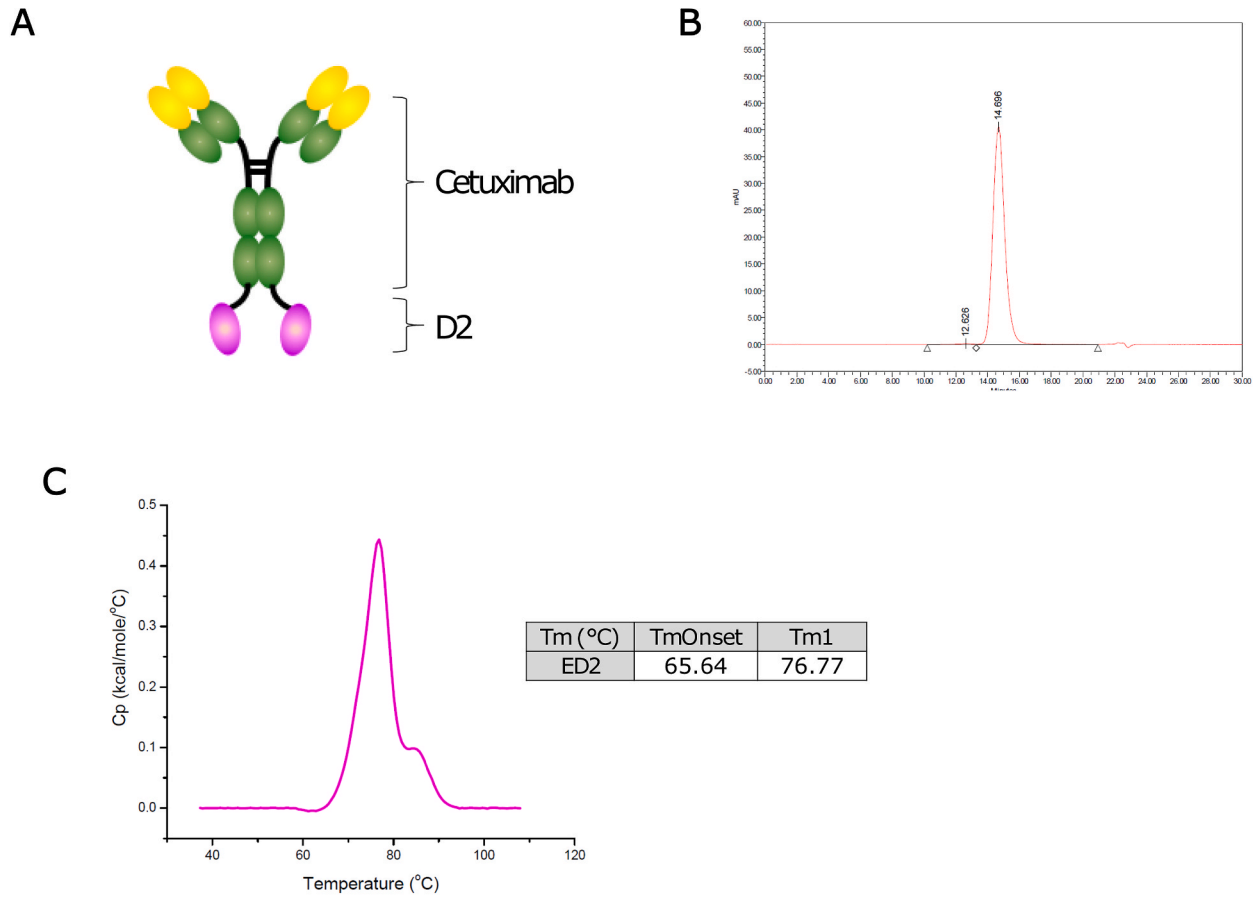

Fig. 1. Construction of the *anti*-EGFRxD2 bispecific fusion protein (ED2). (A) Schematics of the ED2 structure. (B) SEC chromatography showed that the purity of the ED2 monomer after one-step protein A purification was greater than 98%. (C) The differential scanning calorimetry (DSC) graph of ED2 showed that ED2 had a T_{onset} (the temperature at the onset of melting) of 65.64 °C and a Tm (melting temperature) of 76.77 °C.

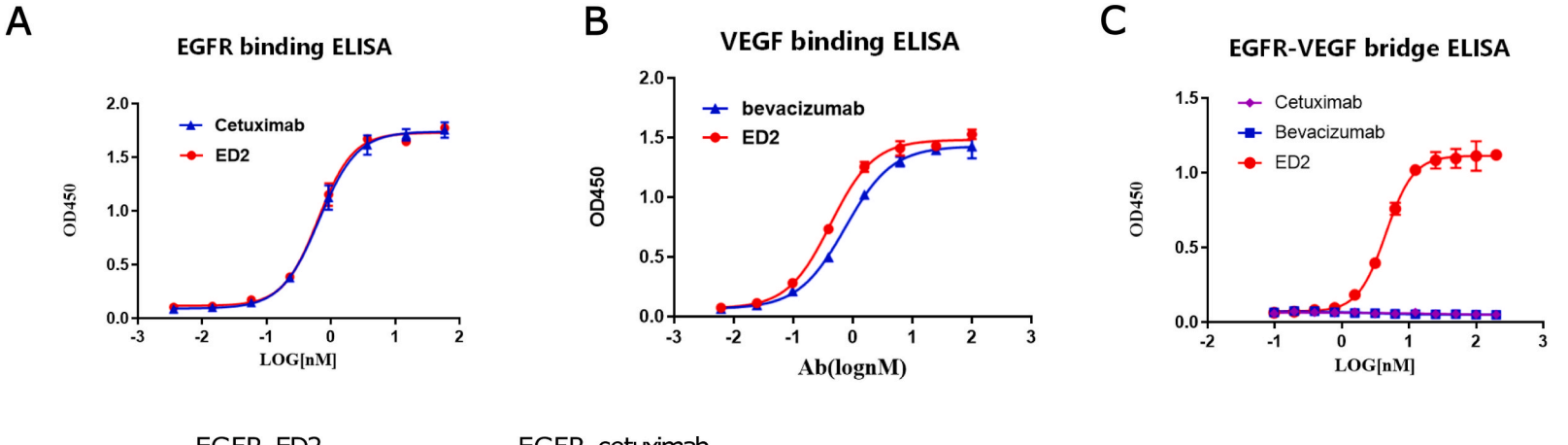

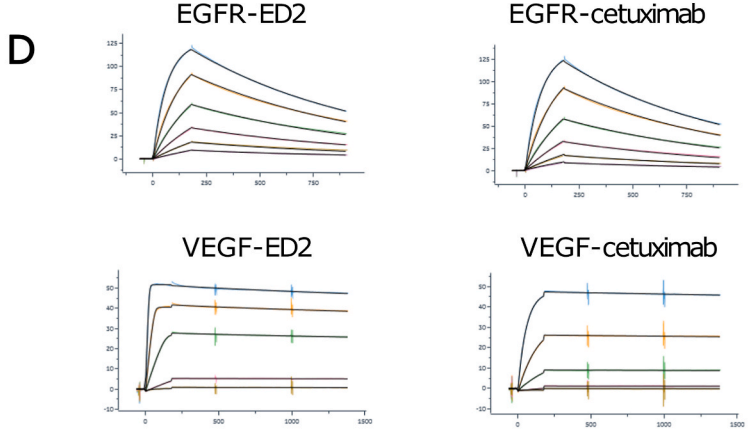

Protein Name	Target	K_{on} ($M^{-1}s^{-1}$)	K_{off} (s^{-1})	KD (M)
ED2	EGFR	1.23E+06	1.19E-03	9.69E-10
Cetuximab		1.22E+06	1.30E-03	1.07E-09
ED2	VEGF	2.86E+07	8.32E-05	2.91E-12
Bevacizumab		1.77E+06	2.76E-05	1.56E-11

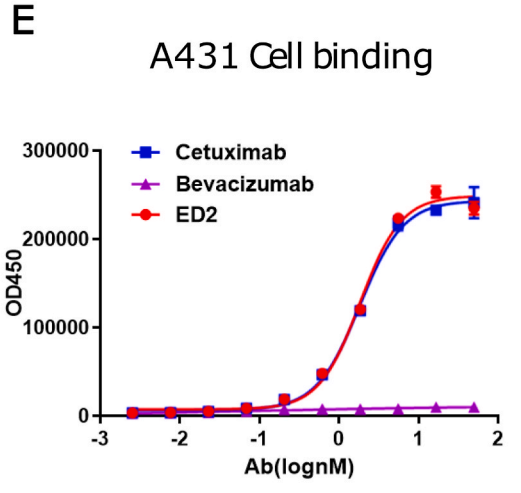

Fig. 2. ED2 simultaneously bound to EGFR and VEGF. (A) The binding affinity of ED2 for EGFR was measured by ELISA. Cetuximab was used as the positive control. (B) The binding affinity of ED2 for VEGF was measured by ELISA and compared to that of bevacizumab and cetuximab. (C) The ability of ED2 to simultaneously bind EGFR and VEGF was measured by bridging ELISA, where VEGF was coated on the plates, followed by the addition of serially diluted antibodies in the presence of EGFR. (D) The equilibrium dissociation constants (KDs) of ED2 for EGFR and VEGF were measured by Biacore and compared to those of the mAb counterparts cetuximab and bevacizumab, respectively. (E) The ability of ED2 to bind to A431, an EGFR-overexpressing cancer cell line, was measured by FACS and compared to that of cetuximab.

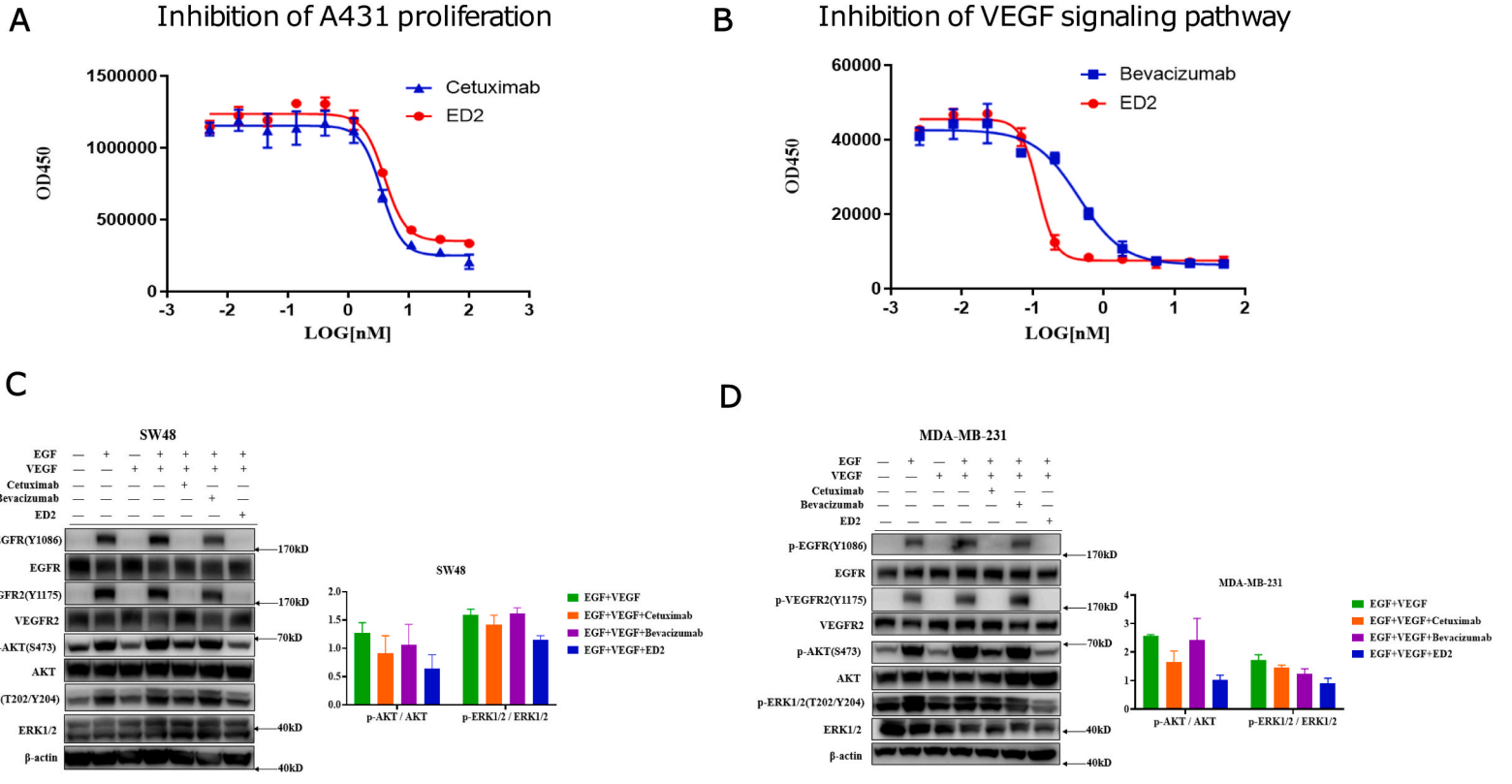

Fig. 3. ED2 inhibited the proliferation of A431 tumor cells and a KDR-expressing cell line. (A) ED2 inhibited the proliferation of EGFR-overexpressing A431 cancer cells as potently as cetuximab. (B) ED2 inhibited the proliferation of a KDR-overexpressing cell line (Promega) as potently as bevacizumab. (C and D) SW48 and MDA-MB-231 cells were treated with EGF (20 ng/ml), VEGF (400 ng/ml) or the combination of EGF with VEGF (20 ng/ml + 400 ng/ml) in the absence or presence of indicated antibodies (50 M each), respectively. + represents "added"; - represents "not included". Cell lysates were prepared and western blotting was performed for the following markers: *p*-EGFR (Y1086), Y1086-phosphorylated EGFR; EGFR, total EGFR as the loading control for *p*-EGFR; *p*-VEGFR2 (Y1175), Y1175-phosphorylated VEGFR2; VEGFR2, total VEGFR2 as the loading control for *p*-VEGFR2; *p*-AKT (S473), S473-phosphorylated AKT; AKT, total AKT as the loading control for *p*-AKT; *p*-ERK1/2 (T202/Y204), phosphorylated ERK1/2; ERK1/2, total ERK1/2 as the loading control for *p*-ERK1/2; β-actin serves as the loading control for whole cell lysates. *p*-AKT and *p*-ERK1/2 levels of samples treated with EGF + VEGF, or EGF + VEGF in the presence of indicated antibodies, respectively, were quantified and normalized to total AKT or ERK1/2. The original pictures can be found in supplemental materials.

step purification with protein A chromatography (Fig. 1b). In addition, differential scanning calorimetry (DSC) confirmed that ED2 had the desired melting temperatures of 65.6 °C for the onset peak (T_{onset}) and 76.8 °C for the first peak (Tm1), indicating that the protein had favorable physicochemical properties for further development (Fig. 1c).

3.2. ED2 could simultaneously bind to EGFR and VEGF

We next examined the ability of ED2 to bind to its targets EGFR and VEGF. The ELISA results showed that ED2 was able to bind to EGFR with an EC_{50} of 0.63 nM, which was comparable to the EC_{50} value of 0.66 nM for the parental monoclonal antibody (mAb) cetuximab (Fig. 2a). We examined its binding to VEGF, and ED2 also showed a high affinity for VEGF with an EC_{50} value of 0.42 nM, which was 2-fold better than the 0.75 nM of the *anti*-VEGF mAb bevacizumab (Fig. 2b). Furthermore, ED2 could bridge the two target proteins with an EC_{50} value of 4.52 nM, indicating that there was no steric hindrance that could interrupt the simultaneous interaction of ED2 with EGFR and VEGF. In contrast, the two mAbs cetuximab and bevacizumab failed to do so (Fig. 2c). We confirmed the high binding capacity of ED2 for both targets with Biacore, which showed that the equilibrium dissociation constants (KDs) of ED2 for VEGF and EGFR were 0.97 nM and 2.9 pM, respectively, on par with those of the mAb counterparts (Fig. 2d). To ensure that ED2 could target tumor cells, we examined the ability of ED2 to bind to A431 cells, an EGFR-overexpressing human epidermoid carcinoma cell line. FACS analysis showed that ED2 strongly bound to A431 cells with an EC_{50} value of 1.84 nM, which was consistent with that of the parental mAb cetuximab (1.83 nM; Fig. 2e). These data suggest that the *anti*-EGFR-D2 fusion protein can effectively interact with its targets.

3.3. ED2 potently inhibited target cell growth through inhibition of AKT and ERK1/2 signaling

Next, to confirm that ED2 could inhibit EGFR-expressing tumor cell and endothelial cell proliferation by blocking EGFR and VEGFR signaling, we examined the effects of ED2 on the proliferation of A431 tumor cells and a KDR-overexpressing cell line (Promega). Treatment of EGFR-expressing A431 tumor cells with ED2 significantly inhibited the proliferation of A431 cells with an IC_{50} value of 3.98 nM, which was comparable to the IC_{50} value of 3.56 nM of the parental mAb cetuximab (Fig. 3a). In addition, treatment of KDR-expressing cells with ED2 exhibited superior inhibitory effects on the proliferation of human endothelial cells with an EC_{50} value of 0.12 nM. Compared with that of the *anti*-VEGF mAb bevacizumab, whose IC_{50} value was 0.45 nM, ED2-mediated inhibition of HUVEC growth was approximately 4-fold stronger than that of bevacizumab (Fig. 3b).

Since AKT and ERK1/2 are the downstream targets of the EGFR signaling pathway, we next examined the effects of ED2 on the activation of AKT and ERK1/2. EGF clearly activated EGFR, VEGFR2 signaling as well as their downstream AKT and ERK1/2 signaling in SW48 and MDA-MB-231 cells, as shown by the phosphorylation of EGFR at Y1086, VEGFR2 at Y1175, AKT at S473 and ERK1/2 at T202/Y204 (Fig. 3c and d). As expected, the combination of EGF with VEGF further enhanced the phosphorylation of AKT at S473 (*p*-AKT) and ERK1/2 at T202/Y204 (*p*-ERK1/2) relative to the two growth factors alone. Addition of cetuximab or bevacizumab in the presence of both EGF and VEGF reduced *p*-AKT and pERK1/2 to levels that are comparable to those activated by VEGF or EGF alone,

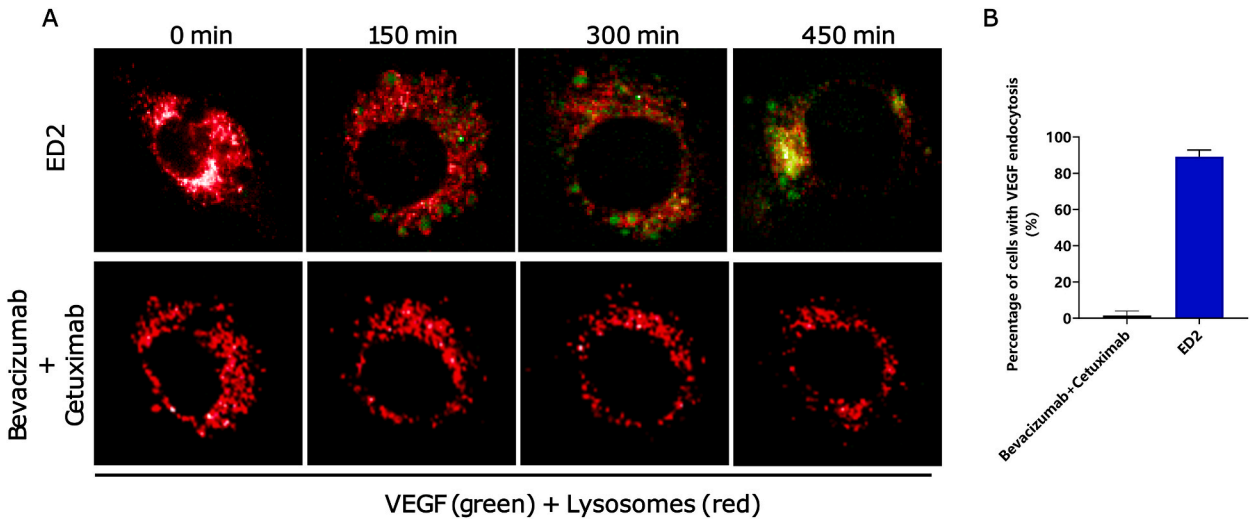

Fig. 4. ED2 could mediate the uptake of soluble VEGF by cells through internalization for lysosome-dependent degradation. (A) Time-lapse movie frames (top panel) showing the uptake of VEGF (green) into cells by ED2-induced internalization. Once inside the cells, VEGF was then gradually translocated to lysosomes (red), where it formed yellow patches (green + red) and disappeared thereafter. Time-lapse movie frames (bottom panel) showing that the combination of the two mAb counterparts cetuximab and bevacizumab failed to bring soluble VEGF into cells. Red: LysoTracker Red DND-99, Green: Alexa Fluor™ 488 NHS Ester. (B) The number of cells treated with ED2 ($n > 100$) that had VEGF uptake was compared with that of cells treated with the combination of the parental mAbs ($n > 100$). (For interpretation of the references to color in this figure legend, the reader is referred to the Web version of this article.)

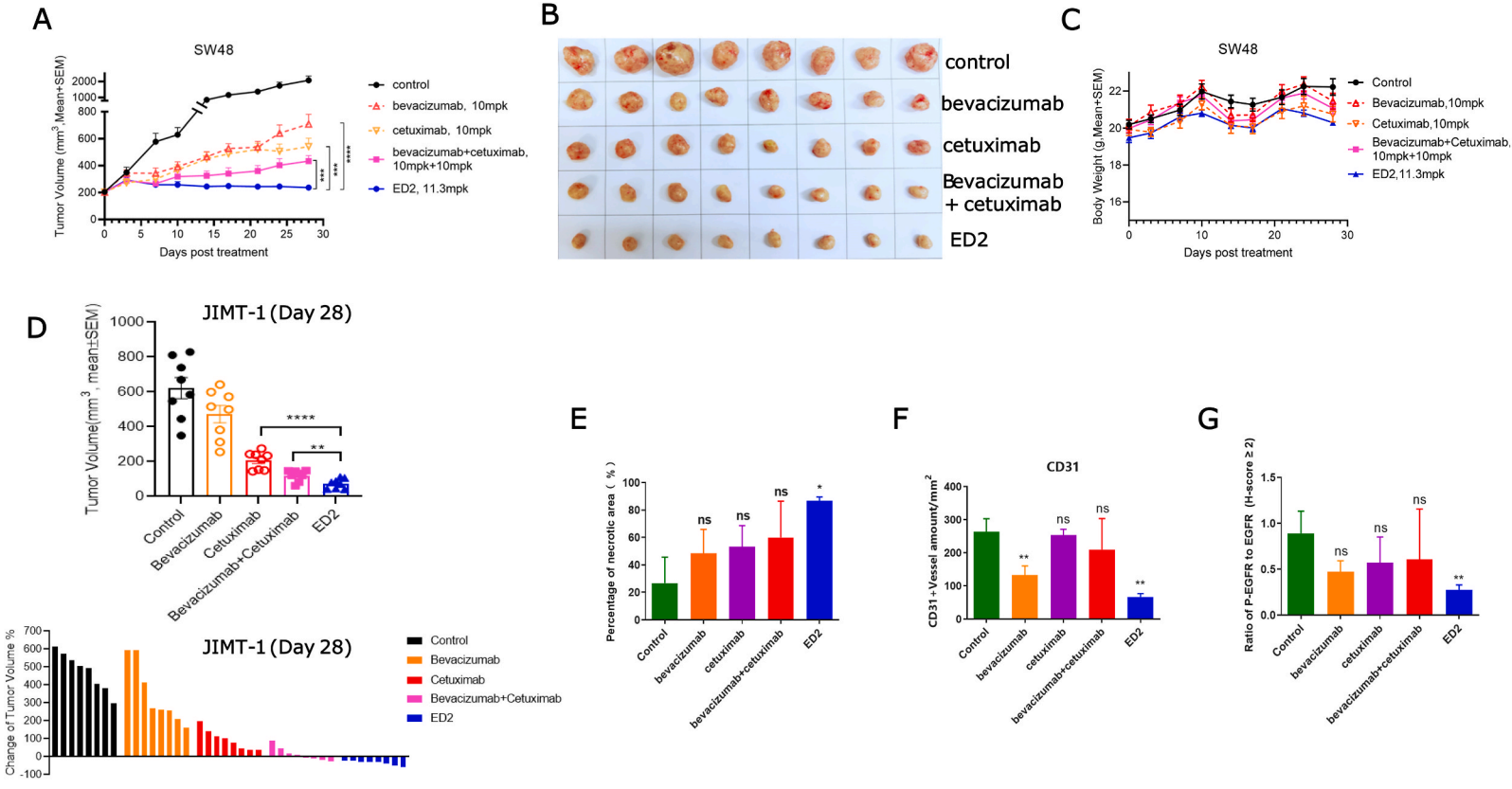

Fig. 5. ED2 exhibited potent antitumor effects *in vivo*. (A) A control (black dot), ED2 (blue dot), bevacizumab (red triangle), cetuximab (yellow triangle) or the combination of bevacizumab with cetuximab (pink square) were i.p. injected into mice bearing SW48 tumors at the indicated doses. Tumor volumes (mm^3) were measured at the indicated time points. Mean ± SEM. ***$p < 0.001$ and ****$p < 0.0001$. (B) Photographs of tumors in the indicated groups. (C) The mouse body weights of each treatment group were measured at the indicated time points. (D) 10 mg/kg control, 10 mg/kg ED2, 10 mg/kg bevacizumab, 10 mg/kg cetuximab or the combination of bevacizumab (10 mg/kg) with cetuximab (10 mg/kg) were i.p. injected into mice bearing JIMT-1 tumors, separately. Tumor volumes (mm^3) were measured on day 28. Mean ± SEM. **$p < 0.01$ and ****$p < 0.0001$. Changes of individual tumor volumes from baseline were shown at the bottom. (E) The necrotic areas of tumors in each treatment group were measured and plotted as percentage of the total tumor. *$p < 0.05$ and NS stands for "Not Significant". (F) Blood vessels were identified by CD31 staining and the number of CD31 positive vessels of each treatment group were measured and compared. **$p < 0.01$ and NS stands for "Not Significant". (G) The amount of tumor cells that did not undergo necrosis and were strongly stained for pEGFR (H-score ≥2) were normalized with that of EGFR-positive tumor cells. The normalized pEGFR signals (ratios of pEGFR/EGFR) were compared between groups. **$p < 0.01$ and NS stands for "Not Significant". (For interpretation of the references to color in this figure legend, the reader is referred to the Web version of this article.)

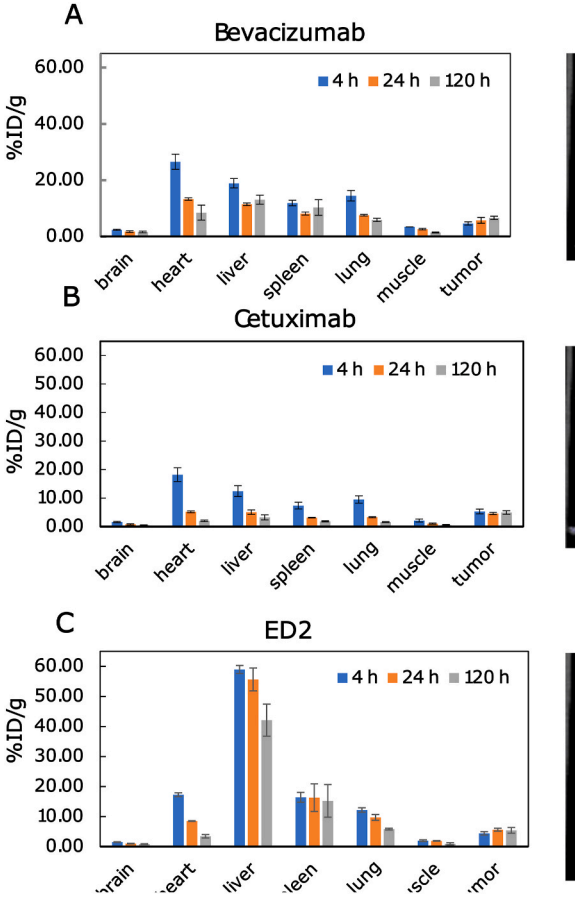

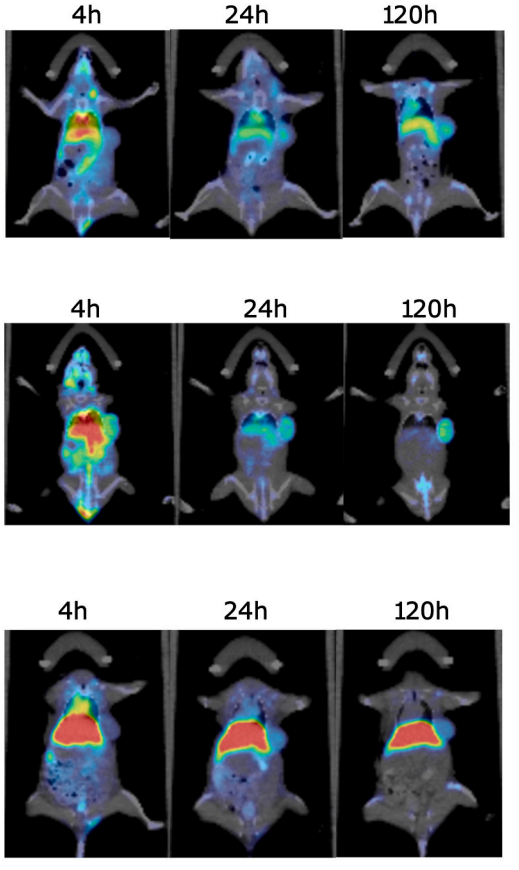

Tissue/ Body fluid	%ID/g (Mean ± SD), n=3		
	4 h	24 h	120 h
brain	2.37 ± 0.21	1.73 ± 0.31	1.63 ± 0.29
heart	26.54 ± 2.68	13.30 ± 0.45	8.48 ± 2.65
liver	18.91 ± 1.67	11.46 ± 0.45	13.09 ± 1.60
spleen	11.89 ± 0.97	8.13 ± 0.54	10.30 ± 2.76
lung	14.48 ± 1.85	7.56 ± 0.28	5.89 ± 0.60
muscle	3.42 ± 0.03	2.62 ± 0.23	1.43 ± 0.15
tumor	4.62 ± 0.57	5.73 ± 1.04	6.61 ± 0.60

Tissue/ Body fluid	%ID/g (Mean ±SD), n=3		
	4 h	24 h	120 h
brain	1.63 ±0.22	0.79 ±0.21	0.52 ±0.10
heart	18.23 ±2.43	5.19 ±0.32	2.03 ±0.26
liver	12.46 ±1.89	5.07 ±0.79	3.23 ±0.89
spleen	7.37 ±1.19	3.14 ±0.13	1.84 ±0.19
lung	9.50 ±1.29	3.32 ±0.19	1.58 ±0.16
muscle	2.12 ±0.53	1.05 ±0.19	0.61 ±0.11
tumor	5.31 ±0.82	4.59 ±0.37	4.95 ±0.62

Tissue/ Body fluid	%ID/g (Mean ±SD), n=3		
	4 h	24 h	120 h
brain	1.51 ±0.10	0.99 ±0.09	0.87 ±0.09
heart	17.27 ±0.64	8.53 ±0.11	3.46 ±0.56
liver	58.94 ±1.36	55.66 ±3.80	42.10 ±5.36
spleen	16.42 ±1.65	16.30 ±4.60	15.21 ±5.42
lung	12.19 ±0.73	9.72 ±0.97	5.85 ±0.30
muscle	1.99 ±0.28	1.89 ±0.10	0.95 ±0.36
tumor	4.42 ±0.57	5.65 ±0.48	5.42 ±0.95

Fig. 6. ED2 rapidly accumulated in tumors to a degree that was comparable to its mAb counterparts in vivo. The %ID/g of ED2 (A), bevacizumab (B) and cetuximab (C) in the indicated tissues was measured at the indicated time points after intravenous injection.

respectively. Interestingly, ED2 in the presence of both EGF and VEGF further reduced *p*-AKT and pERK1/2 compared to those treated with cetuximab or bevacizumab alone in both cell lines, indicating that ED2 has stronger inhibitory effects on signaling pathways that are required for tumor cell growth than its mAb counterparts (Fig. 3c and d). These results are consistent with the observation in our in-vivo studies (see below), where we saw more necrotic cells, stronger suppression of CD31 vascular vessels and the phosphorylation of EGFR in tumors in the ED2 treatment group than in the two mAb treatment groups.

3.4. ED2 in complex with VEGF was internalized in response to binding to EGFR and directed to lysosomes

The Binding of cetuximab to EGFR on the surface of cells induces internalization of the mAb [33]. We then reasoned that extracellular VEGF bound to the bifunctional fusion protein could be taken into cells in response to the binding of ED2 to EGFR, which would direct VEGF to lysosomes for subsequent degradation [34]. To test this hypothesis, we filmed the uptake of VEGF165-488 (VEGF labeled in green) in solution into A431 tumor cells in the presence of ED2 and monitored the translocation of VEGF165-488 to lysosomes (dyed in red) within tumor cells (Fig. 4). Soluble VEGF gradually appeared in tumor cells following the addition of ED2 and then accumulated intracellularly in lysosomes over time (Fig. 4a and b, supplemental movie 1). In contrast, no soluble VEGF was taken into tumor cells in the presence of the mAbs bevacizumab and cetuximab during the experiment, indicating that the uptake of VEGF by tumor cells was mediated by ED2 (Fig. 4a and b, supplemental movie 2).

3.5. ED2 potently inhibited tumor growth in a xenografted colorectal tumor model

We next evaluated the antitumor effects of ED2 *in vivo*. We used an SW48 xenograft model to measure the efficacy of the fusion protein on colorectal tumors. Consistent with previous studies [35], 10 mg/kg cetuximab suppressed 75% of SW48 tumor growth on day 30 after treatment. Injection of 10 mg/kg bevacizumab alone suppressed approximately 65% of tumor growth. Further up to 80% of tumor growth inhibition could be achieved when the combination of bevacizumab and cetuximab was applied at equal molar concentrations (10 mg/kg each). Importantly, ED2 was more potent in suppressing tumor growth than the combination of the two mAbs in equal molar doses, indicating that the bifunctional fusion protein had additive antitumor activities that its mAb counterparts lacked (Fig. 5a and b). Notably, no apparent toxicity associated with ED2 was observed, as the animal body weights remained approximately unchanged throughout the course of the treatment (Fig. 5c). The superior antitumor activity of ED2 was again supported by the JIMT-1 model, where ED2 exhibited significantly more potent suppression of JIMT-1 tumor growth than the combination of cetuximab with bevacizumab with all tumor sizes being reduced from baseline in the ED2 treatment group (Fig. 5d).

Immunohistochemical (IHC) staining was used to assess tumor histology in each treatment group. We first noticed that in addition to having the smallest volumes among all treatment groups, up to 87% of ED2-treated tumors underwent necrosis. In contrast, only 27% and 60% necrosis were observed in the control and mAb combination groups, respectively, supporting the finding that ED2 was more potent in inhibiting tumor growth than the combination of its mAb counterparts (Fig. 5e). We next analyzed tumor blood vessels by CD31 staining, since one of the mechanisms of action of ED2 is to inhibit vascular formation by blocking VEGFR signaling. As expected, the number of blood vessels was significantly reduced in tumors that were treated with ED2 in comparison with those treated with the mAb counterparts either alone or in combination, indicating that the inhibitory effects of ED2 on blood vessel formation in EGFR-overexpressing tumors cannot be replicated by simply combining the mAbs (Fig. 5f). Furthermore, we measured the suppression of EGFR activation in each treatment group with EGFR phospho-Y1173 staining (pEGFR), given that ED2 can block EGFR signaling. Since the tumor necrotic areas could not be stained for pEGFR, positive pEGFR staining was only measured in the nonnecrotic areas of tumors. Intriguingly, treatment of tumors with ED2 substantially attenuated the activation of EGFR via phosphorylation, since only tumor cells treated with ED2 showed significantly weaker pEGFR staining (H-score $\geq$2) than cells in the control group (Fig. 5g), again suggesting that ED2 exhibited stronger antitumor activities than its mAb counterparts.

3.6. ED2 rapidly accumulated in tumors to a degree that was comparable to its mAb counterparts in mice

To further elucidate how ED2, which is a novel tumor-associated antigen (TAA)-targeted molecule, is distributed in the body compared to its mAb counterparts, we determined the tissue distribution of ED2 and the two mAbs bevacizumab and cetuximab in mice. The three proteins were labeled with ^{89}Zr, and their *in vivo* tissue distribution was monitored with a micro-PET/CT imaging system. After I.V. injection, bevacizumab rapidly accumulated in SW48 tumors, with a 4.6% injected dose per gram of tissue (%ID/g) achieved at 4 h. With time, more bevacizumab gradually accumulated in tumors, resulting in 5.7% at 24 h and 6.6% at 120 h. Over the course of bevacizumab treatment, 82.2% ID/g in 7 tissues, including the brain, heart, liver, spleen, lung, kidney and tumor tissues, at 4 h postinjection was sequentially reduced to 50.5% at 24 h and 47.4% at 120 h (Fig. 6a). In contrast, cetuximab quickly reached the maximum concentration of 5.3% ID/g in tumors at 4 h and was persistently 4.6% at 24 h and 4.9% at 120 h. However, 56.62% ID/g in these 7 tissues at 4 h postinjection was sequentially reduced to 23.2% at 24 h and 14.8% at 120 h, indicating that cetuximab had a faster tissue clearance rate than bevacizumab (Fig. 6b). With respect to ED2, which contains both EGFR- and VEGF-targeting moieties, 4.4%, 5.7% and 5.4% ID/g were observed at 4 h, 24 h and 120 h after injection, respectively, indicating that the time required for ED2 to reach a maximum concentration in tumors was between that of cetuximab and bevacizumab. Surprisingly, the animal bodies tended to accumulate more ED2 in these 7 tissues than the other two mAbs, with an initial 112.7% ID/g at 4 h, followed by a gradual reduction to 98.7% at 24 h and 73.9% at 120 h. Notably, ED2 substantially accumulated in the liver (58.9% ID/g at 4 h) and was hardly removed at 24 h (55.7% ID/g), whereas both bevacizumab and cetuximab accumulated in the heart (26.5% and 18.2% ID/g, respectively) at 4 h, and bevacizumab was quickly removed by half (13.3% ID/g), while cetuximab was removed by more than 3-fold (5.2% ID/g) at 24 h

(Fig. 6c). These data suggest that all three molecules had different tissue distribution profiles, which might be explained by their distinct targeting properties.

Given that ED2 primarily accumulated in the liver and may possibly affect liver functions, we next did blood biochemical tests for liver functions. In line with the animal body check results, all six tests examined for the level of Albumin (ALB), alkaline phosphatase (ALP), alanine transaminase (ALT), aspartate aminotransferase (AST), Cholinesterase (CHE) and total protein (TP) in the blood appeared to be normal in all antibody treatment groups, including ED2, compared to that of the control group, indicating that ED2 did not provoke liver malfunctions despite its substantial accumulation in the liver (Fig. 7a–f).

4. Discussion

In this study, we used D2 as a VEGF-targeting domain combined with cetuximab to construct a dual functional fusion protein that could simultaneously inhibit EGFR and VEGF signaling. D2, which is the second domain of VEGFR1, can fold properly by itself and be produced easily. Using D2 as a VEGF-targeting moiety in a bispecific format has the following theoretical merits: (1) The molecular weight of D2 is approximately half of that of a single-chain Fv (scFv). Thus, a fusion protein that consists of two copies of D2 connected to the C-terminus of an IgG is approximately 25 KD smaller in size than that of the one with two copies of scFvs. For a therapeutic agent targeting solid tumors, the smaller size might facilitate the penetration of the drug into tumors [36]. (2) D2 is a native human protein and might have no or low immunogenicity when administered into a human body. (3) D2 binds tightly to VEGF with a KD of 2.9 pM, which is comparable to that of bevacizumab (15 pM). Thus, D2 can effectively block the binding of VEGF to KDR and inhibit VEGF-dependent HUVEC growth. (4) D2 is a naturally occurring protein domain and has favorable physicochemical properties for drug development [21]. For these reasons, the construction of a D2-based multispecific molecule might be a promising strategy to integrate *anti*-VEGF function and improve antitumor therapy.

ED2 retained the ability to bind both EGFR and VEGF with pM affinities and was also able to bind to EGFR-overexpressing cancer cells (A431) as effectively as the parental mAb cetuximab. Importantly, ED2 exhibited strong inhibitory effects on the growth of A431 tumor cells and HUVEC in vitro. These results can at least partly attribute to the fact that ED2 has stronger inhibitory effects on the AKT and ERK1/2 signaling pathways, since Western blotting showed that tumor cells treated with ED2 have less *p*-AKT and *p*-ERK1/2 than cells treated with the mAb counterparts alone. Since it was shown that cetuximab could induce the internalization of the cetuximab/

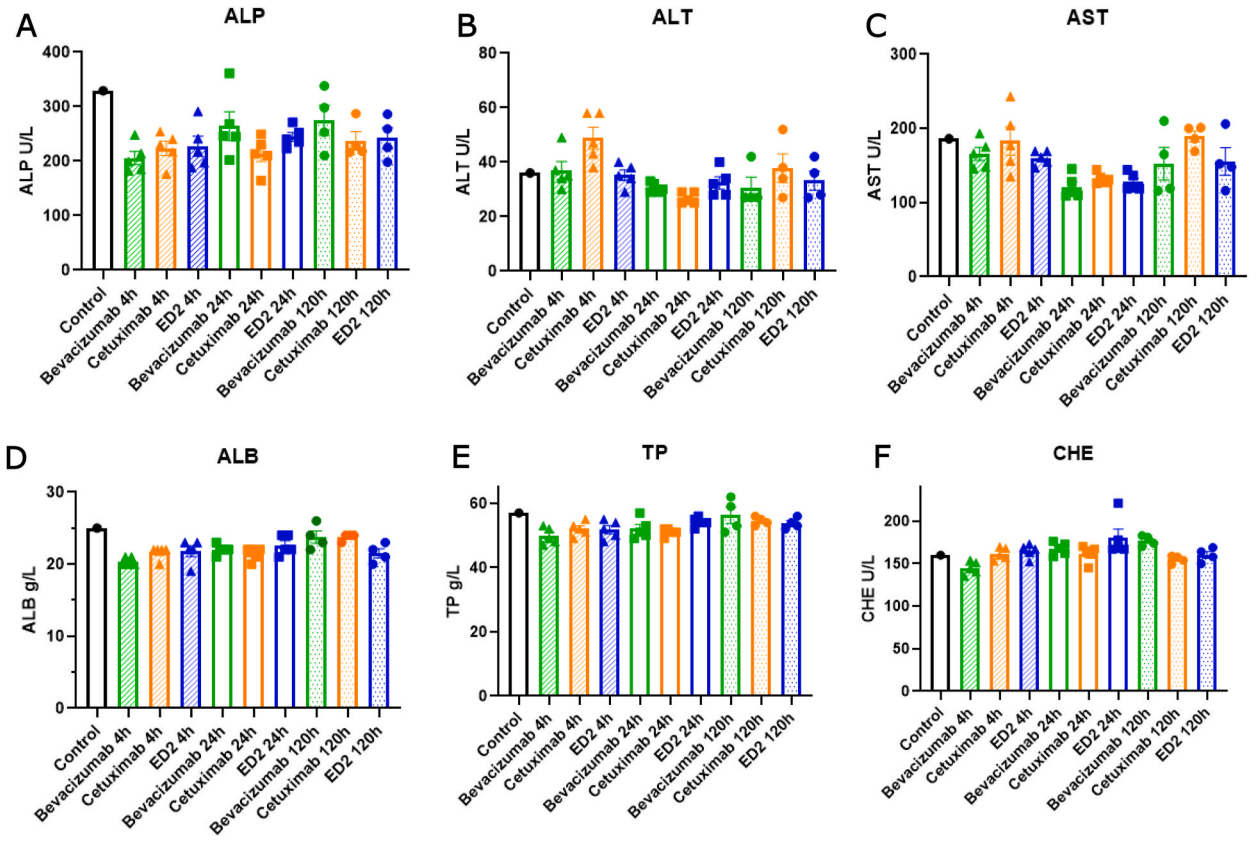

Fig. 7. ED2-treated animals exhibited normal liver functions. Total 6 tests, including ALP (A), ALT (B), AST (C), ALB (D), TP (E) and CHE (F) were performed for samples treated with indicated antibodies at indicated time points by an independent contract research organization (CRO) (Shanghai Model Organisms Center Inc., Shanghai).

receptor complex into cells after binding to EGFR [33], extracellular VEGF may be captured by ED2 via D2 and be taken into cells and degraded intracellularly by lysosomes. To test this hypothesis, we tracked the movement of soluble VEGF in the presence of A431 tumor cells after the addition of ED2 and showed that VEGF in solution could enter tumor cells shortly after the addition of ED2 and gradually accumulated in intracellular lysosomes, whereas combining bevacizumab and cetuximab failed to induce the internalization of VEGF in solution. These results suggest that VEGF might be removed in tumor cells through binding to ED2, and this reduction in the extracellular VEGF concentration could extended vascular suppression in the tumor microenvironment and prolong the inhibition of tumor growth.

Indeed, the superior antitumor efficacy of ED2 was confirmed in xenograft tumor models using two types of EGFR-expressing cancer cell lines: SW48 (colon) or JIMT-1 (breast). In support of the promising in vitro binding and cell-based assays, ED2 exhibited superior antitumor activity compared to either of its two mAb counterparts, bevacizumab and cetuximab in these mouse models. Importantly, ED2 exhibited stronger inhibitory effects on tumor growth (tumor shrinkage could be seen) than the combination of bevacizumab and cetuximab, indicating that the fusion protein possesses synergistic antitumor activities that mAbs lack. IHC staining confirmed that ED2 exhibited stronger tumor killing (necrosis), VEGF/VEGFR blockade and EGFR blockade than the combination of bevacizumab and cetuximab. Intriguingly, pEGFR could be only detected in nonnecrotic areas of tumors, suggesting that a basal EGFR signaling may be required to maintain SW48 tumor cells survival. Indeed, the weak staining of pEGFR (H-score = 1) was observed in tumor nonnecrotic areas among all treatment groups. In contrast, tumor cells with strong pEGFR staining (H-score $\geq$2) were significantly reduced in tumors treated with ED2 than with the control, indicating that ED2 was more potent in the suppression of EGFR activation through phosphorylation than the other agents. It is plausible that while adding the two mAbs can effectively block VEGF and EGFR signaling separately at the same time, ED2 might offer additional effect that can support its antitumor efficacies, such as facilitating VEGF internalization for degradation.

To further understand how ED2 works in animals as an agent that can not only be directed to and kill tumors via EGFR but also inhibit angiogenesis by inhibiting VEGF signaling, we tracked the tissue distribution of ED2 in mice, as well as that of its two mAb counterparts, after the proteins were labeled with ^{89}Zr. As expected, cetuximab quickly accumulated in EGFR-overexpressing tumors and peaked within 4 h posttreatment. Although bevacizumab and ED2 also quickly translocated to tumors after administration, with over 70% of the total amount in tumors within 4 h, the two of them took 120 and 24 h to reach the maximum concentrations in tumors, respectively. The longest time for bevacizumab to translocate to tumors was consistent with the broad distribution of VEGF in the body [37], which also explains why ED2, which targets both EGFR and VEGF, takes a longer time than cetuximab but a shorter time than bevacizumab to accumulate in tumors. Intriguingly, the total amount of the drugs that could be taken up by tumors was approximately the same for all three agents, indicating that the uptake of the three proteins by tumors was saturated at approximately 5% ID/g, which may reflect the amount of available EGFR and VEGF in the tumor microenvironment. Interestingly, the clearance of cetuximab from tissues other than tumors was faster than that of bevacizumab and ED2, most likely because EGFR is more specifically expressed in tumors than in normal tissues, whereas VEGF is more universally expressed in various tissues and keeps the two VEGF-targeting proteins from being cleared. These findings emphasize the importance of balancing the occupancy of targets of interest in tumors and normal tissues through the design of dosing schedules for agents that have multiple targeting moieties. Importantly, ED2 more potently inhibited the growth of tumors than bevacizumab and cetuximab alone or in combination, despite the similar amount of the 3 proteins that accumulated in tumors, indicating that ED2 might have synergistic antitumor activities that simply combining bevacizumab and cetuximab does not achieve.

In summary, we devised a novel VEGF trap that could be directed to the tumor environment by targeting EGFR on tumors. ED2 was constructed by connecting D2 to the C-terminus of cetuximab, which enabled the protein to bind VEGF and EGFR effectively and inhibited the tumor cell growth induced by the two signaling pathways. In addition to its blockade activities, ED2 could capture soluble VEGF for degradation in tumor cells through EGFR internalization. As a result, ED2 exhibited superior antitumor activity compared to that of the combination of bevacizumab and cetuximab, although these agents were equally effective in accumulating in tumors. Taken together, we provide a new strategy to improve the treatment of EGFR-overexpressing cancers.

Author contribution statement

Lan Deng: Conceived and designed the experiments; Analyzed and interpreted the data. Lihua Wang: Performed the experiments; Analyzed and interpreted the data. Jinzhao Zhang; Le Zhao: Performed the experiments. Yun Meng; Jidai Zheng; Wei Xu: Contributed reagents, materials, analysis tools or data. Zhenping Zhu: Conceived and designed the experiments. Haomin Huang: Conceived and designed the experiments; Analyzed and interpreted the data; Wrote the paper.

Data availability statement

Data will be made available on request.

Declaration of competing interest

The authors declare that they have no known competing financial interests or personal relationships that could have appeared to influence the work reported in this paper.

Appendix A. Supplementary data

Supplementary data to this article can be found online at https://doi.org/10.1016/j.heliyon.2023.e16922.

References

[1] D.A. Sabbah, R. Hajjo, K. Sweidan, Review on epidermal growth factor receptor (EGFR) structure, signaling pathways, interactions, and recent updates of EGFR inhibitors, Curr. Top. Med. Chem. 20 (10) (2020) 815–834.
[2] S. Sigismund, D. Avanzato, L. Lanzetti, Emerging functions of the EGFR in cancer, Mol. Oncol. 12 (1) (2018) 3–20.
[3] N. Normanno, et al., Epidermal growth factor receptor (EGFR) signaling in cancer, Gene 366 (1) (2006) 2–16.
[4] P.M. Boland, W.W. Ma, Immunotherapy for colorectal cancer, Cancers 9 (5) (2017).
[5] C.S. Grasso, et al., Genetic mechanisms of immune evasion in colorectal cancer, Cancer Discov. 8 (6) (2018) 730–749.
[6] S. Alfieri, S. Cavalieri, L. Licitra, Immunotherapy for recurrent/metastatic head and neck cancer, Curr. Opin. Otolaryngol. Head Neck Surg. 26 (2) (2018) 152–156.
[7] S. Watanabe, et al., Clinical responses to EGFR-tyrosine kinase inhibitor retreatment in non-small cell lung cancer patients who benefited from prior effective gefitinib therapy: a retrospective analysis, BMC Cancer 11 (2011) 1.
[8] R. Pirker, et al., EGFR expression as a predictor of survival for first-line chemotherapy plus cetuximab in patients with advanced non-small-cell lung cancer: analysis of data from the phase 3 FLEX study, Lancet Oncol. 13 (1) (2012) 33–42.
[9] R. Bianco, et al., Intrinsic and acquired resistance to EGFR inhibitors in human cancer therapy, Endocr. Relat. Cancer 12 (Suppl 1) (2005) S159–S171.
[10] F. Morgillo, et al., Primary and acquired resistance to anti-EGFR targeted drugs in cancer therapy, Differentiation 75 (9) (2007) 788–799.
[11] A.M. Viloria-Petit, R.S. Kerbel, Acquired resistance to EGFR inhibitors: mechanisms and prevention strategies, Int. J. Radiat. Oncol. Biol. Phys. 58 (3) (2004) 914–926.
[12] J.J. Lin, et al., Five-year survival in EGFR-mutant metastatic lung adenocarcinoma treated with EGFR-TKIs, J. Thorac. Oncol. 11 (4) (2016) 556–565.
[13] C. Ding, et al., Combined application of anti-VEGF and anti-EGFR attenuates the growth and angiogenesis of colorectal cancer mainly through suppressing AKT and ERK signaling in mice model, BMC Cancer 16 (1) (2016) 791.
[14] X. Le, et al., Dual EGFR-VEGF pathway inhibition: a promising strategy for patients with EGFR-mutant NSCLC, J. Thorac. Oncol. 16 (2) (2021) 205–215.
[15] F.Z. Shahneh, et al., Tumor angiogenesis and anti-angiogenic therapies, Hum. Antibodies 22 (1–2) (2013) 15–19.
[16] N. Ferrara, VEGF-A: a critical regulator of blood vessel growth, Eur. Cytokine Netw. 20 (4) (2009) 158–163.
[17] X. Li, U. Eriksson, Novel VEGF family members: VEGF-B, VEGF-C and VEGF-D, Int. J. Biochem. Cell Biol. 33 (4) (2001) 421–426.
[18] N. Ferrara, H.P. Gerber, J. LeCouter, The biology of VEGF and its receptors, Nat. Med. 9 (6) (2003) 669–676.
[19] C.J. Peach, et al., Molecular pharmacology of VEGF-A isoforms: binding and signalling at VEGFR2, Int. J. Mol. Sci. 19 (4) (2018).
[20] J. Holash, et al., VEGF-Trap: a VEGF blocker with potent antitumor effects, Proc. Natl. Acad. Sci. U. S. A. 99 (17) (2002) 11393–11398.
[21] Y. Shen, et al., A bi-functional antibody-receptor domain fusion protein simultaneously targeting IGF-IR and VEGF for degradation, mAbs 7 (5) (2015) 931–945.
[22] S. Lee, et al., Phase II study of ramucirumab in advanced biliary tract cancer previously treated by gemcitabine-based chemotherapy, Clin. Cancer Res. 28 (11) (2022) 2229–2236.
[23] L. Micheli, et al., VEGF-A/VEGFR-1 signalling and chemotherapy-induced neuropathic pain: therapeutic potential of a novel anti-VEGFR-1 monoclonal antibody, J. Exp. Clin. Cancer Res. 40 (1) (2021) 320.
[24] N. Ferrara, K.J. Hillan, W. Novotny, Bevacizumab (Avastin), a humanized anti-VEGF monoclonal antibody for cancer therapy, Biochem. Biophys. Res. Commun. 333 (2) (2005) 328–335.
[25] S.P. Ivy, J.Y. Wick, B.M. Kaufman, An overview of small-molecule inhibitors of VEGFR signaling, Nat. Rev. Clin. Oncol. 6 (10) (2009) 569–579.
[26] S.M. Ferrari, et al., Sunitinib in the treatment of thyroid cancer, Curr. Med. Chem. 26 (6) (2019) 963–972.
[27] C. Ciccarese, et al., Efficacy of VEGFR-TKIs plus immune checkpoint inhibitors in metastatic renal cell carcinoma patients with favorable IMDC prognosis, Cancer Treat Rev. 100 (2021), 102295.
[28] Y. Itatani, et al., Resistance to anti-angiogenic therapy in cancer-alterations to anti-VEGF pathway, Int. J. Mol. Sci. 19 (4) (2018).
[29] R.S. Herbst, et al., Efficacy of bevacizumab plus erlotinib versus erlotinib alone in advanced non-small-cell lung cancer after failure of standard first-line chemotherapy (BeTa): a double-blind, placebo-controlled, phase 3 trial, Lancet 377 (9780) (2011) 1846–1854.
[30] K. Nakagawa, et al., Ramucirumab plus erlotinib in patients with untreated, EGFR-mutated, advanced non-small-cell lung cancer (RELAY): a randomised, double-blind, placebo-controlled, phase 3 trial, Lancet Oncol. 20 (12) (2019) 1655–1669.
[31] X. Sun, et al., Multi-scale agent-based brain cancer modeling and prediction of TKI treatment response: incorporating EGFR signaling pathway and angiogenesis, BMC Bioinf. 13 (2012) 218.
[32] W. Liang, et al., Multiscale modeling reveals angiogenesis-induced drug resistance in brain tumors and predicts a synergistic drug combination targeting EGFR and VEGFR pathways, BMC Bioinf. 20 (Suppl 7) (2019) 203.
[33] C. Berger, I.H. Madshus, E. Stang, Cetuximab in combination with anti-human IgG antibodies efficiently down-regulates the EGF receptor by macropinocytosis, Exp. Cell Res. 318 (20) (2012) 2578–2591.
[34] P. Saftig, J. Klumperman, Lysosome biogenesis and lysosomal membrane proteins: trafficking meets function, Nat. Rev. Mol. Cell Biol. 10 (9) (2009) 623–635.
[35] L. Li, et al., Tumor-targeting anti-EGFR x anti-PD1 bispecific antibody inhibits EGFR-overexpressing tumor growth by combining EGFR blockade and immune activation with direct tumor cell killing, Transl. Oncol. 14 (1) (2021), 100916.
[36] M.S. Dennis, et al., Imaging tumors with an albumin-binding Fab, a novel tumor-targeting agent, Cancer Res. 67 (1) (2007) 254–261.
[37] C. Kut, F. Mac Gabhann, A.S. Popel, Where is VEGF in the body? A meta-analysis of VEGF distribution in cancer, Br. J. Cancer 97 (7) (2007) 978–985.